PROCEEDINGS OF SPIE

SPIEDigitalLibrary.org/conference-proceedings-of-spie

From Doppler to speckle variance measurements in optical coherence tomography

Adrian Podoleanu, Sophie Caujolle, Manuel Marques, Ramona Cernat, Ranjan Rajendram, et al.

Adrian Podoleanu, Sophie Caujolle, Manuel Marques, Ramona Cernat, Ranjan Rajendram, Adrian Bradu, "From Doppler to speckle variance measurements in optical coherence tomography

," Proc. SPIE 10831, Seventh International Conference on Lasers in Medicine, 108310D (10 August 2018); doi: 10.1117/12.2283530

SPIE.

Event: Seventh International Conference on Lasers in Medicine, 2017, Timisoara, Romania

Invited Paper

From Doppler to speckle variance measurements in optical coherence tomography

Adrian Podoleanu[*a], Sophie Caujolle[a], Manuel Marques[a], Ramona Cernat[a], Ranjan Rajendram[b], Adrian Bradu[a]

[a]Applied Optics Group, School of Physical Sciences, University of Kent, Kent CT2 7NH, U.K; [b]Moorfields Eye Hospital, University College London Institute of Ophthalmology, London EC1V 9EL, U.K

ABSTRACT

A short-review of optical coherence tomography (OCT) technologies employed to evaluate and image flow and tiny movements is presented. Over the time, the progress of OCT from time domain to spectral (Fourier) domain SD-OCT has led to new approaches in measuring flow and tissue (object) vibration. In the present document, several procedures are presented of what is known today as OCTA, used to visualize tiny vessels in the human retina and replacing the need for injection in angiography. These methods are now extended to measurements of minuscule spatial variations due to action potential, cell division or tissue deformation in elastography.

Keywords: Optical Coherence Tomography, multiple imaging, motion estimation, optical flow, speckle variance

1. INTRODUCTION

Since the early age of the OCT technology [1,2], structural images described by B-scan images (cross section images) or C-scan images (*en-face* images) have proven their usefulness in the clinic, a lot of work being done to enhance the quality of images as well as their interpretation. Work on the hardware led to increasing the axial and transversal resolution. Recent work on the software led to refocusing and dispersion correction. There is also a trend towards functional assessment by using for example spectroscopic OCT, Optical Coherence Elastography, etc.

OCT angiography (OCTA) is one of these modalities which maps the vascularity of a biological sample, especially used on the human retina. Age-related macular degeneration, glaucoma and diabetic retinopathy are the three main reasons of visual field loss and blindness. They have a direct impact on blood vessels by reducing the retinal blood flow and inducing choroidal neovascularization. Currently, the gold standard to diagnose and follow the evolution of the disease are semi-invasive methods such as Fluorescein Angiography and Indocyanine Green Angiography. OCTA presents the advantage to be non-invasive and requires no injection of contrast agents.

SD-OCT has been combined with Doppler imaging [3] to acquire images of blood flow in skin [4] and human retina [5-7] that allow angiography imaging with no dye. Doppler based methods provide the magnitude and direction of flow. To reduce the sensitivity of measurement to undesired phase instabilities, a joint spectral and time domain OCT [8] method has been introduced. A different method is based on fluctuation measurements that employ variations in phase between successive images. Phase-variance OCT between successive B-scans allowed mapping of micro-vasculature without quantitative flow information [9]. By calculating the squared intensity difference between successive tomograms [10], the flow against static tissue can be contrasted. Intensity based methods are insensitive to electronic trigger jitter and therefore are better suited to swept source OCT systems.

In a previous work, we presented simultaneous interrogation of flow at multiple depths separated by a spatial interval which is adjustable from zero to values which are less, larger, or much larger than the coherence length of the optical source. The key to this method was the use of recirculating loops in both reference and sample arms of a low-coherence interferometer. A similar configuration was previously reported for delivering several C-scan OCT images from different depths simultaneously in a Drosophila melanogaster larvae [11], as well as from the human eye in vivo [12].

Seventh International Conference on Lasers in Medicine, edited by Darinca Carmen Todea, Adrian Gh. Podoleanu, Virgil-Florin Duma, Proc. of SPIE Vol. 10831, 108310D

2. DOPPLER MEASUREMENTS

Doppler measurements were performed using an in-housebuilt time-domain OCT system based on single mode fibers. A schematic diagram of the set-up is presented in Fig. 1, where light from a broadband optical source (Lumen Photonics 1530-1560 nm) is amplified by an erbium doped optical amplifier (Amonics AEDFA-PA-35-B-FA) and split into a main sample and reference arms by a directional coupler DC 1 (50/50 splitting ratio). In each arm of the interferometer, a separate optical loop (1 and 2), with an adjustable path length is built (Interface Optics 1 and 2, which consist of microscope objectives and translation stages). Each loop incorporates an acousto-optic frequency shifter (AOFS) that shifts the optical frequency upward by the frequency of the driving signal. Two semiconductor optical amplifiers (SOA1 and SOA2, QPhotonics QSOA-1050) are incorporated into the two loops to compensate for losses. In order to protect the SOAs from stray reflections, optical isolators Is1a,b and Is2a,b are placed at their inputs and outputs. Multiple depths within the flow can be simultaneously interrogated, depth separated by the difference between the optical path lengths of the two loops, OPD_L, difference which can be adjusted by the Interface Optics 1 and 2 incorporated in the loops.

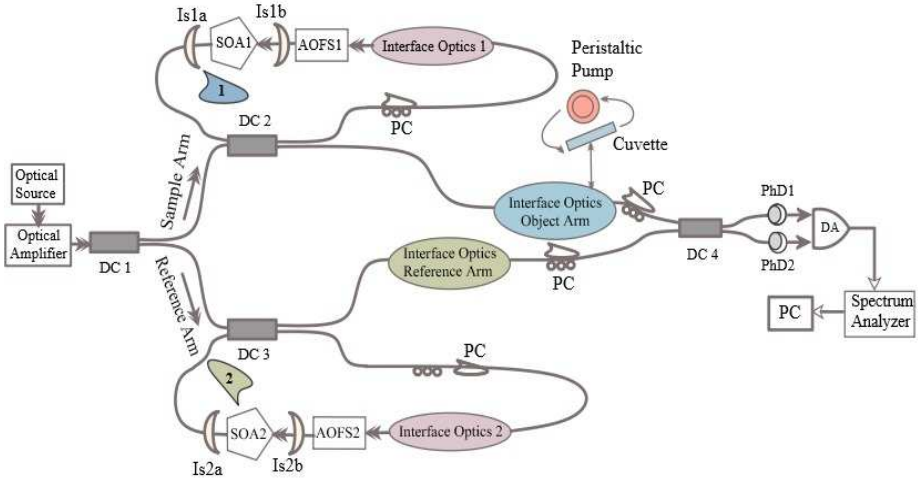

Fig. 1 Schematic diagram of the time-domain OCT system used to perform Doppler measurements: DC1-4 directional couplers, PC: polarization controllers, Is1a, Is1b, Is2a, Is2b: optical isolators, SOA1,2: semiconductor optical amplifiers, AOFS1,2: acousto-optic frequency shifters, PD1,2: photo-detectors, DA: differential amplifier

The injection of light into the loops and the reinjection of the amplified light into the main loop take place at the directional couplers DC2 and DC3. For every pass of light through the two loops, the optical frequency is shifted by f_S (f_R). Let us define the OPD as the difference between the path length in the reference arm and the path length in the sample arm. Essential for following the flow direction is to define Δf as the difference of frequencies, f_S-f_R, i.e., of frequencies of signals applied to the AOFS in the sample path and to the AOFR in the reference arm. This means that a positive Doppler shift, f_D, leads to an increase of the beating recorded by the photo-detected signal: $\delta f = \Delta f + f_S = f_S - f_R + f_D$. The multiple waves from the reference path interfere with the multiple waves from the sample path at the directional coupler DC4, producing a frequency beat at $|f_S - f_R| = p\Delta f$, where p is the number of re-circulations of light in the two loops. The DC4 output signals are sent to a balanced photo-detector unit, consisting of two photo-detectors (PhD1 and PhD2). Two different spectrum analyzers are used to measure the spectrum of the detected signal (Hewlett Packard 3561A for low frequency range (1 Hz –100 kHz) and a Hewlett Packard 8590A for high-frequency range (10 kHz–1.5 GHz)). To perform Doppler measurements flow is generated by a peristaltic pump (Gilson Minipuls 3), that pumps an Intralipid solution (Phospholipid-stabilized soybean oil, 20%, emulsion, Sigma Aldrich) at a minimum flow velocity of 0.64 µl/s through a 1 mm thickness quartz flow cuvette (n=1.43, Starna Scientific, Type 45 Flow Cells). For the cuvette and the connecting pipes used, a calibration was performed by measuring the volume of fluid flown in a given time, obtaining 6.47 µl/s for a 1 rpm on the pump.

Figure 2a shows the screens of the RF spectrum analyzer displaying the spectrum of the photo-detected signal for $\Delta f = 10$ kHz, at a pump speed of 1 rpm to the left, no flow and 1 rpm to the right. The component around 0 Hz (order p= 0) corresponds to the interference of waves originating from the main loop only, that traveled along OPDM while the other peaks at multiples of $\Delta f = 10$ kHz (orders p = 1-5) are generated by interference of similar orders p, of re-circulation waves

in the loops, originating from p axial points from inside the cuvette. In Fig. 2b the frequency shift of each carrier frequency for the situation shown in fig 2a) where pump speed = 1 rpm and Δf = 10 kHz together with their standard deviations is presented. The following measurements where the value of Δf is adjusted to accommodate different flow velocities, with a pump speed from 0.1 rpm to 10 rpm and carrier frequencies of Δf =1 kHz, Δf =10 kHz, and Δf =100 kHz were chosen to be performed. Evaluating the frequency deviations from the rest position for all 5 peaks, a flow profile in the cuvette can be drawn, as shown in Fig. 2(c, d, e) for different pump speeds/velocity flux values (0.64 µl/s, 1.94 µl/s, 3.23 µl/s…64.7 µl/s). The larger the velocity flux and the larger the order p, the wider the peak and the lower the amplitude of the peak. For Δf =100 kHz and s = 10 rpm the 5th order p was of a too small amplitude to be precisely measured (Fig. 2e).

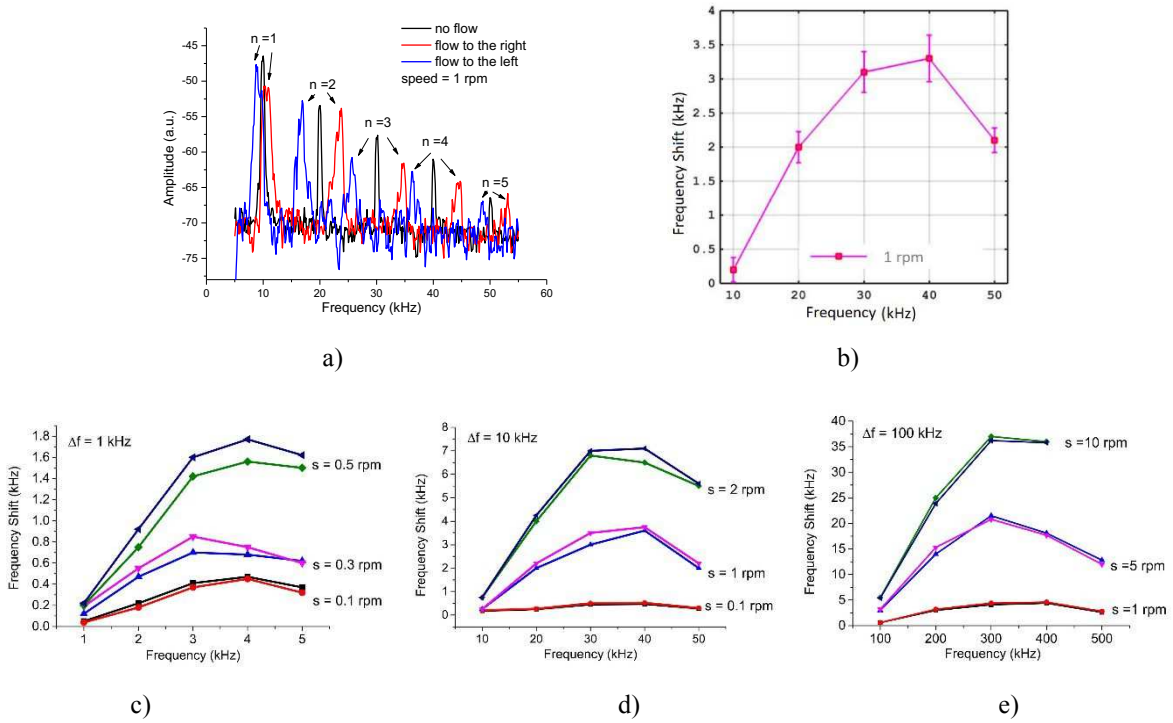

Fig.2 (a) Screen shots of the low frequency spectrum analyzer for a velocity flux of 0 and 1 rpm flow to the left/right. Each component represents the carrier pΔf of an independent measurement channel, where Δf =10 kHz. b) Frequency shift of each carrier frequency for the situation shown in fig 2a) where pump speed = 1 rpm and Δf = 10 kHz together with their standard deviations. (c)–(e) Deviations of each carrier frequency from the no flow situation for several velocity flux values, 0.1, 0.3, 0.5, 1, 2, 5 and 10 rpm, and carrier frequencies of Δf =1 kHz, Δf =10 kHz, and Δf =100 kHz. For each case, two graphs are shown, corresponding to flow to the left and flow to the right.

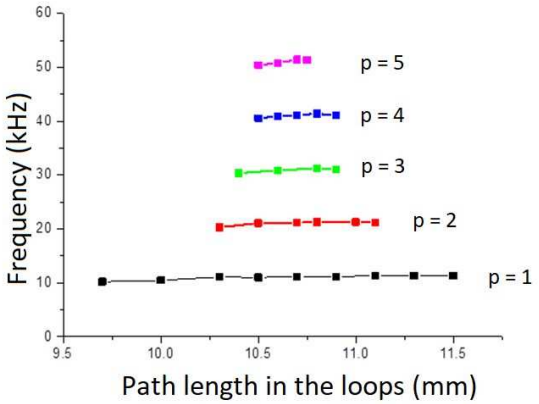

Fig.3 Optical path length in the loops (mm) vs carrier frequency (kHz).

Due to multiple recirculations of the waves in the secondary loops, the larger the number of roundtrips, the smaller the needed OPD variation in the secondary loop to explore the entire flow profile (Fig. 3). OPD was modified, and the frequency shifts were measured for each carrier (corresponding to p =1 to 5 re-circulations of light in the two loops). The extension of the profile measured using waves traversing the loops once, p =1, covers approximately 3 mm, as expected. The other profiles, for p = 2, 3, 4, 5 cover proportionally less.

A calibration by measuring the volume of fluid flown in a given time, obtaining 6.47 µl/s for a 1 rpm on the pump was performed, and we succeeded to record speeds in the range of 0.0358 mm/s to 35.8 mm/s. The maximum speed measurable is determined by the bandwidth. The optimum selection for the Δf value was possible because the velocity order of magnitude was known. In practice however, even if this is not known, measurements could start from the largest Δf allowed by system that is subsequently reduced until a significant shift is seen on the spectrum analyzer. If the choice is incorrect, for example when using a carrier of 1 kHz or 10 kHz for a shift, the carrier is not seen at the right frequency position and aliasing components arise. If by varying the flow velocity, some peaks travel on the analyzer screen in one direction and some others in the opposite direction, this is a clear indication of aliasing that require a larger value Δf.

3. MOTION DETECTION BY OCT

Several methods have been developed using the amplitude or the phase from the optical signal of successive B-scan images [15-20]. All techniques follow the same acquisition protocol, several images, at least two are acquired at the same position in real time (Fig.4). Then, s datasets are reconstructed using Complex Master Slave Interferometry (cMSI) method giving access to the structural images [21,22]. The MS technology proceeds in two steps: the master and the slave ones. During the master step, the system is calibrated by using a flat mirror as object, in the sample arm. Several channeled spectra (minimum two), are acquired for different optical path differences. These sets of spectra, named experimental masks, incorporate non-linearities and unbalanced dispersion in the interferometer. The masks, are then used to infer theoretically as many complex masks as depths needed. Once the set of masks is produced [21], the mirror is replaced by the sample to be imaged. The channeled spectrum at the OCT interferometer output is compared to the full set of complex masks. A comparison operation is initiated at the slave stage of the channeled spectrum with each complex mask.

The functional images are based on structural images. To infer the flow, images from the same position are compared using mathematical operations such as variance or correlation calculation.

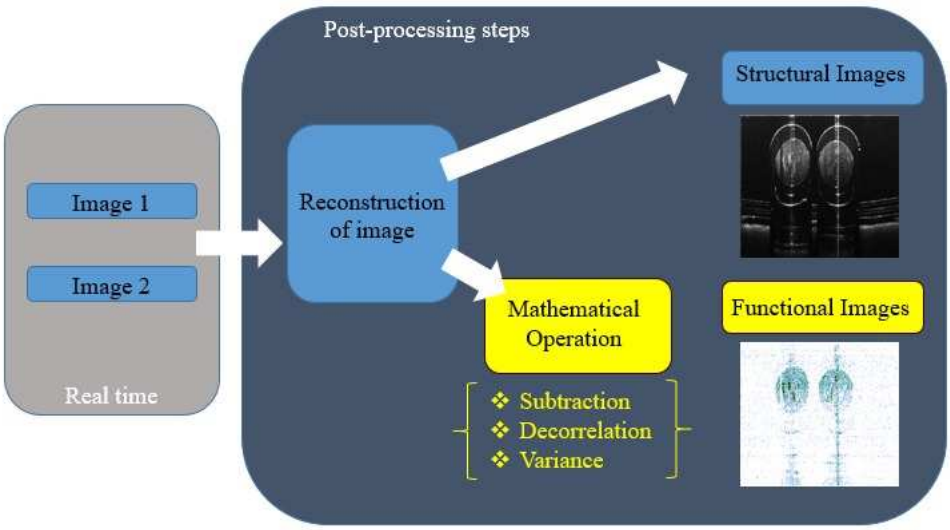

Fig. 4. Acquisition Protocol of structural and functional images. cMSI method gives access direclty to structural images. To obtain functional images, several structural images from the same position are compared using variance or correlation calculation.

The angiography methods are based on mathematical operations such as variance, difference or correlation [15-20] applied totwo main entities: the phase and the amplitude of the modulated optical signal.

$$Variance\ (i,j) = \frac{1}{N}\sum_{q=0}^{N}(x_{i,j,q} - x_{mean})^2$$

$$Difference\ (i,j) = \frac{1}{N}\sum_{q=0}^{N}(x_{i,j,q} - x_{i,j,q-1})$$

$$Correlation\ (i,j) = \frac{1}{N}\sum_{q=0}^{N}\frac{x_{i,j,q}\,.\,x_{i,j,q+1}}{\frac{1}{2}\,({x_{i,j,q}}^2 + {x_{i,j,q+1}}^2)}$$

where x is the amplitude or the phase of the signal, N is the total number of B-scans considered at the same position, (i,j) the axial and lateral coordinate. In the ideal case, only two successive B-scans are enough to create an angiography image. Each OCTA image is "cleaned" using a threshold applied to the values calculated using the above equations, depending on the method chosen. A threshold is chosen to remove noise which presents a high variance value by the fact that it is a random and sometimes, some static features presented too high back reflections. However, this parameter needs to be wisely chosen. If it is too low, some static parts are still visible and if too high, small vessels can be missed. To reduce the value of the threshold while removing the static features, several methods have been investigated based on averaging of several angiography images.

A possible method consists in averaging over several B-scans acquired from the same lateral position. This reduces the noise and draws a more defined vasculature (equivalent increase in the acquisition time and so increase of the amount of red blood cells passing by the imaged area) but it is more sensitive on background motion and it is time consuming. Indeed, for a fixed image size, the time is multiplied by n-1 where n is the number of B-scans at the same position compared to the ideal case.

Another method reported [23] is to split the spectrum into k Gaussian window bands to obtain several spectra from the same lateral position (Fig.5). At each position (x,y), the spectrum (k,n) is compared to the spectrum (k,n+1) where n is the B-scan number at the same scanning position. At the end, we have (2k-1)*(n-1) comparisons. In this way, the number of averaged images is multiplied by a (2k-1) factor achiving the needed average employed by the first method mentioned above. In this way, the oversampling number "n" can be minimized. The acquisition time is reduced while averaging over these 2k-1 angiography images leads to better signal-to-noise ratio of flow detection. However, the axial resolution is impacted and depreciated by a k factor.

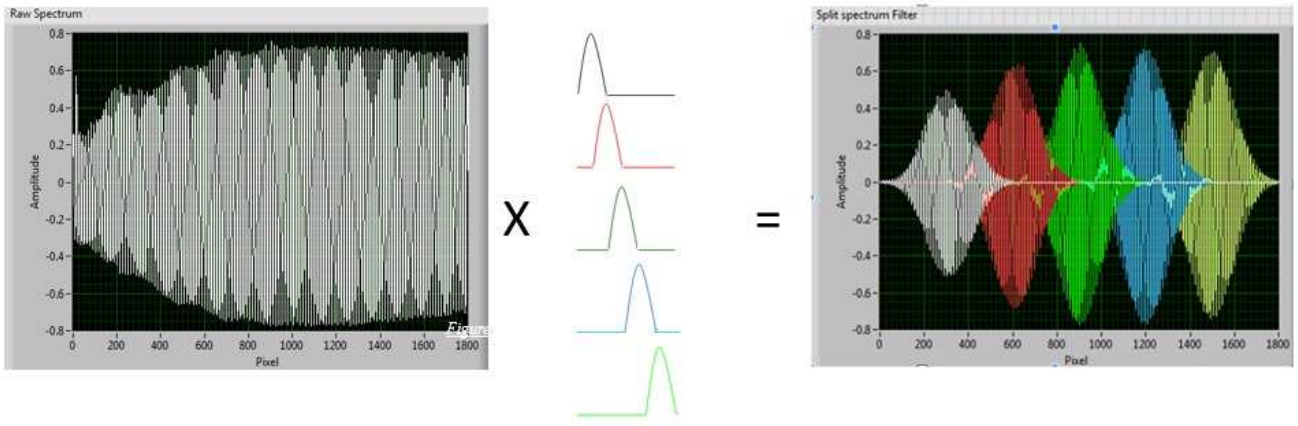

Fig.5 Split spectrum averaging method. Full unprocessed channelled spectrum at the output of the balanced photo-detector (left graph) is multiplied by Gaussian windows to create several spectra. These windowed raw spectra are afterwards used separetly to create B-scan images. After motion detection correction, angiography images are created by averaging.

In figure 6, examples of structural and functional image are shown. The method used was split spectrum amplitude decorrelation angiography (SSADA) [23] where k=3 and n=2. The sample was a tube on the top of a piece of paper flowing

milk using a pump. To have a better visualization of the flowing milk, the functional image is presented in purple on the top of the structural image. Static features can be separated from moving ones.

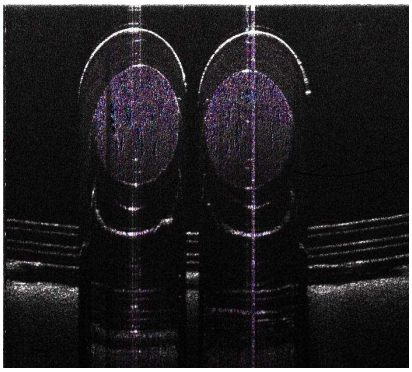

Fig. 6 Structural and functional images of a rubber tube through which milk is flowing. The functional image is colored in purple and superposed to the structural one. The line through the tube is due to saturation and for this reason, shown a wrong value in the correlation calculation.

EMBRYO MONITORING

Angiography means drawing the vessel map and methods mentioned above are mainly used to do this. However, it is important to note that any of such OCTA methods are sensitive to the moving blood inside the vessel. Thus, they can be also applied to detect motion from cells or embryo evolution. A recent article shows the monitoring of an embryo over several hours [24]. Tiny movements inside the embryo were evaluated by calculating the speckle variance between two successive images (*en-face* images). This has allowed to quantify the level of changes within the 3D volume of the embryo and define areas that manifest a certain degree of liveliness. OCTA was proven as a reliable tool in quantifying the embryo lifetime when deprived from suitable environment for their existence.

CONCLUSIONS

In this manuscript, time and spectral imaging modalities have been presented. A scalable time domain multiple path configuration was presented, that allows simultaneous interrogation of an intralipid flow at several axial depths in a vessel. The set-up is reconfigurable in respect to differential distance and speed range measurable. Measurements were presented for different frequency shift Δf values to accommodate different velocity ranges. The other method described refers to spectral domain, where cMSI is used in the signal processing. Here the range can only be changed by altering the sweeping of the swept source or reading speed of the camera in the spectrometer.

Acknowledgements
RC, and AP are supported by the NIHR Biomedical Research Centre at Moorfields Eye Hospital NHS Foundation Trust and the UCL Institute of Ophthalmology. AP, AB and MM acknowledge EPSRC Grants (REBOT) EP/N019318/1 and EP/N019229/1. SC and AP acknowledge Marie Curie Initial Training Network UBAPHODESA 607627. AP also acknowledges the Royal Society Wolfson Research Merit Award and the ERC ADASMART' 754695.

REFERENCES

[1] M.R. Hee, C.A. Puliafito, C. Wong, J.S. Duker, E. Reichel, J.S. Schuman, E.A Swanson and J.G. Fujimoto, "Optical coherence tomography of macular holes," Ophthalmology, **102**(5), 748-756, (1995).
[2] W. Drexler, U. Morgner, F.X. Kärtner, C. Pitris, S.A. Boppart, X.D. Li, E.P. Ippen, and J.G. Fujimoto, "In vivo ultrahigh-resolution optical coherence tomography," Opt. lett., **24**(17), 1221-1223, (1999).

[3] R. G. Liu and Z. Chen, “Phase-resolved Doppler optical coherence tomography,” in Selected Topics in Optical Coherence Tomography, G. Liu Ed. Rijeka, Croatia: InTech, 2012.
[4] Y. Zhao et al., “Phase-resolved optical coherence tomography and optical Doppler tomography for imaging blood flow in human skin with fast scanning speed and high velocity sensitivity,” Opt. Lett., vol. 25, no. 2, pp. 114–116, Jan. 2000.
[5] B. R. White et al., “In vivo dynamic human retinal blood flow imaging using ultra-high-speed spectral domain optical Doppler tomography,” Opt. Exp., vol. 11, no. 25, pp. 3490–3497, Dec. 2003.
[6] S. Makita, Y. Hong, M. Yamanari, T. Yatagai, and Y. Yasuno, “Optical coherence angiography,” Opt. Exp., vol. 14, no. 17, pp. 7821–7840, Aug. 2006.
[7] B. Baumann et al., “Total retinal blood flow measurement with ultrahigh speed swept source/Fourier domain OCT,” Biomed. Opt. Exp., vol. 2, no. 6, pp. 1539–1552, Jun. 2011.
[8] G. Liu and Z. Chen, “Phase-resolved Doppler optical coherence tomography,” in Selected Topics in Optical Coherence Tomography, G. Liu Ed. Rijeka, Croatia: InTech, 2012.
[9] M. Szkulmowski, A. Szkulmowska, T. Bajraszewski, A. Kowalczyk, and M. Wojtkowski, “Flow velocity estimation using joint spectral and time domain optical coherence tomography,” Opt. Exp., vol. 16, no. 9, pp. 6008–6025, Apr. 2008.
[10] D. Y. Kim et al., “In vivo volumetric imaging of human retinal circulation with phase-variance optical coherence tomography,” Biomed. Opt. Exp., vol. 2, no. 6, pp. 1504–1513, Jun. 2011.
[11] C. Blatter et al., “In situ structural and microangiographic assessment of human skin lesions with high-speed OCT,” Biomed. Opt. Exp., vol. 3, no. 10, pp. 2636–2646, Oct. 2012.
[12] L. Neagu, A. Bradu, L. Ma, J. W. Bloor, and A. G. Podoleanu, “Multiple-depth en face optical coherence tomography using active recirculation loops,” Opt. Lett., vol. 35, no. 13, pp. 2296–2298, Jul. 2010.
[13] J. A. Rogers, A. Bradu, and A. G. Podoleanu, “Polarization maintaining multiple-depth en face optical coherence tomography system using active re-circulation loops in the non-stationary state,” Opt. Exp., vol. 20, no. 28, pp. 29196–29209, Dec. 2012.
[14] R. Cernat, A. Bradu, R. Rajendram, A. Podoleanu Simultaneous measurement of flow at several depths using multiple active paths in a low-coherence interferometer. *IEEE Photonics Journal* **7** (3):0-0. ISSN 1943-0655. 2015
[15] D. Ruminski, B.L. Sikorski, D. Bukowska, M. Szkulmowski, K. Krawiec, G. Malukiewicz, L. Bieganowski and M. Wojtkowski, “OCT angiography by absolute intensity difference applied to normal and diseased human retinas,” Biomed. Opt. Express, **6**(8) (2015)
[16] A. Federici, H.S. Gutierrez da Costa, J. Ogien, A.K. Ellerbee and A. Dubois, “Wide-field, full-field optical coherence microscopy for high axial-resolution phase and amplitude imaging,” Appl. Optics, **54**(27) (2015)
[17] I. Gorczynska, J.V. Migacz, R.J. Zawadzhi, A.G. Capps and J.S. Werner, “Comparison of amplitude-decorrelation, speckle variance and phase-variance OCT angiography methods for imaging the human retina and choroid,” Biomed. Opt. Express, **7**(3) (2016)
[18] M.S. Mahmud, D.W. Cadotte, B. Vuong, C. Sun, T.W. Luk, A. Mariampillai and V.X. Yang, “Review of speckle and phase variance optical coherence tomography to visualize microvascular networks,” J. Biomed. Opt., **18**(5) (2013)
[19] A. Mariampillai, M.K.K. Leung, M. Jarvi, B.A. Standish, K. Lee, B.C. Wilson, A. Vitkin and V.X.D. Yang, “Optimized speckle variance OCT imaging of microvasculature,” Opt. Lett., **35**(8), (2010).
[20] Y. Huang, Q. Zhang, M.R. Thorell, L. An, M.K. Durbin, M. Laron, U. Sharma, G. Gregori, P.J. Rosenfeld and R.K. Wang, "Swept-source OCT angiography of the retinal vasculature using intensity differentiation-based optical microangiography algorithms," OSLI Retina, **45**(5), 382-389, (2014).
[21] S. Rivet, M. Maria, A. Bradu, T. Feuchter, L. Leick and A. Podoleanu, “Complex master slave interferometry,” Opt. Express, **24**(3), 2885, (2016).
[22] A. Bradu, S. Rivet and A. Podoleanu, “Master/slave interferometry - ideal tool for coherence revival swept source optical coherence tomography “Biomed. Opt. Express, **7**, 2453-2468 (2016).
[23] Y. Jia, O. Tan, J. Tokayer, B. Potsaid, Y. Wang, J.J. Liu, M.F. Krauss, H. Subhash, J.G. Fujimoto, J. Hornegger and D. Huang, “Split-spectrum amplitude decorrelation angiography with optical coherence tomography” Opt. Express, **20**(4) (2012)
[24] S. Caujolle, R. Cernat, G. Silvestri, M. J. Marques, A. Bradu, T. Feuchter, G. Robinson, D. K. Griffin, and A. Podoleanu, "Speckle variance OCT for depth resolved assessment of the viability of bovine embryos," Biomed. Opt. Express 8, 5139-5150 (2017).